Journal of Alloys and Compounds, 195 (1993) 235–238
JALCOM 7456

$\vec{a}$ axis laser ablated superconducting YBCO thin films Growth mechanism on MgO substrate

J.F. Hamet, B. Mercey, M. Hervieu, B. Blanc-Guilhon, G. Poullain and B. Raveau

Laboratoire de Cristallographie et Sciences des Matériaux - CRISMAT - ISMRa - Université de Caen - URA CNRS 1318
Boulevard du Maréchal Juin - 14050 CAEN Cedex, FRANCE

Abstract :

We have successfully grown $\vec{a}$-axis oriented YBCO superconducting thin films on MgO substrates. The growth mechanism has been studied by T.E.M. At 650°C a cubic perovskite is formed with a_p // a_{MgO}. Then a strained tetragonal $\vec{a}$ axis oriented phase is formed with c = 3a exhibiting a marquetry-like contrast. At 750°C, a [1$\bar{1}$0] axis oriented perovskite is formed whose lattice exhibits a rotation with respect to MgO but also a tilting of $[CuO_2]_\infty$ layers with the substrate plane. Introduction of oxygen at this temperature leads to an $\vec{a}$-axis oriented orthorhombic perovskite with a poorly crystallized interface layer. An almost perfect $\vec{a}$-axis thin film is achieved after a slow cooling down to room temperature. A zero resistance superconducting transition temperature of 89 K has been measured.

1. Introduction

The use of pulsed laser ablation for the deposition of YBCO thin films has been used successfully by different authors for the fabrication of $\vec{c}$-axis oriented thin films i.e. with the $\vec{c}$ axis perpendicular to the plane of the substrate [1-4]. Recently, $\vec{a}$ axis YBCO thin films have been grown by A. Inam and T. Hase, and the deposition performed on (100) $LaAlO_3$ and (100) $SrTiO_3$ was interpreted as an epitaxial growth process [5-9]. The recent growth of $\vec{a}$ axis oriented thin films on (100) MgO with excellent characteristic showed the absence of epitaxial mechanism [10]. In this paper the different steps of the growth process are described.

2. Experimental

The films were grown by pulsed laser deposition using a KrF excimer laser (λ = 248 nm). The beam is focused on a stoechiometric $YBa_2Cu_3O_7$ bulk target with an energy close to 2J/cm^2 and a repetition rate of 2 Hz. The deposition rate is around 1 Å/s under an oxygen pressure of 0.2 mbar. For the deposition on MgO single crystals, the "in-situ" thermal conditions are more different from those needed for the deposition of $\vec{c}$ axis films. The deposition is indeed started at 650°C in order to favoured the orientation of the $[CuO_2]_\infty$ layers perpendicular to the substrate (Fig. 1a). Then the temperature is progressively increased to 750°C.

Transmission electron microscopy has been performed with a JEOL 200 CX fitted with an eucentric goniometer (± 60°) and Topcon 2B with a double tilt goniometer operating at 200 kV.

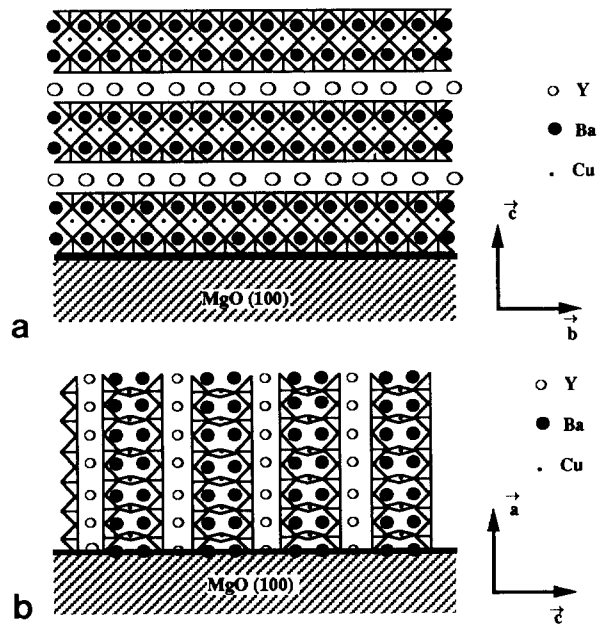

Fig. 1. Orientation of YBCO films with respect to the MgO substrate. (a) c-axis of films perpendicular to the substrate; (b) a-axis of films perpendicular to the substrate.

In order to study the evolution of the thin films structure during the deposition, the films are obtained by "quenching" i.e. by decreasing the temperature as fast as possible as soon as the ablation is stopped. First, a cubic perovskite is formed after 4 min of deposition at 650°C and 0.2 mbar O_2. The electron diffraction (E.D.) pattern (Fig. 2a) shows that the cubic perovskite cell is

0925-8388/93/$06.00

rigorously oriented with respect to the MgO cubic cell i.e. $a_p // a_{MgO}$ with a_p = 3.86 Å. This orientation cannot be attributed to an epitaxial process owing to the large difference between the lattice parameters of YBCO and MgO. After a larger time at 650°C, this cubic disordered phase is replaced by a tetragonal ordered phase whose c parameter is abnormally short (c = 11.58 Å) leading to a c/a ratio = 3. This oxide can be identified as the T_3 phase $YBa_2Cu_3O_{6.8}$ which is not superconductive [11].

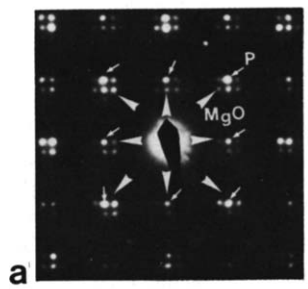

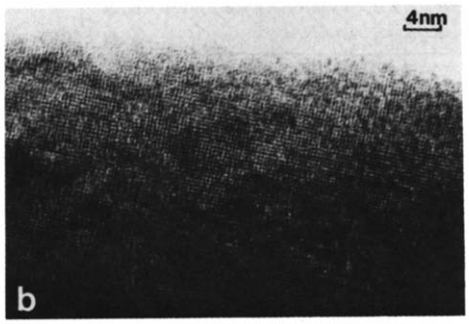

Fig. 2. (a) [001] electron diffraction pattern of the perovskite P (small arrows) with $a_p // a_{MgO}$; (b) high resolution images show a well crystallized film.

The high resolution electron microscope (HREM) image of the tetragonal phase (Fig. 3a); shows that the $\vec{c}$ axis is parallel to the substrate plane. This phase is $\vec{a}$ axis oriented with respect to the substrate and exhibits a marquetry-like contrast (Fig. 3a) with tiny 90° oriented domains (50 Å). From the corresponding electron diffraction patterns (Fig. 3b), a very small rotation (< 3°) of the marquetry structure is sometimes observed with respect of the MgO matrix.

At an higher temperature, 750°C, and the same oxygen pressure the tetragonal marquetry-like structure is transformed into larger domains which exhibit the "1-2-3" orthorhombic symmetry as shown in figure 4. The $\vec{c}$ axis remains parallel to the substrate plane but the $\vec{a}$ (or $\vec{b}$) axis is no more perpendicular to the substrate plane i.e. the $[CuO_2]_\infty$ layers are inclined with respect to this plane. The $[1\bar{1}0]$ direction of the orthorhombic cell is perpendicular to the substrate plane.

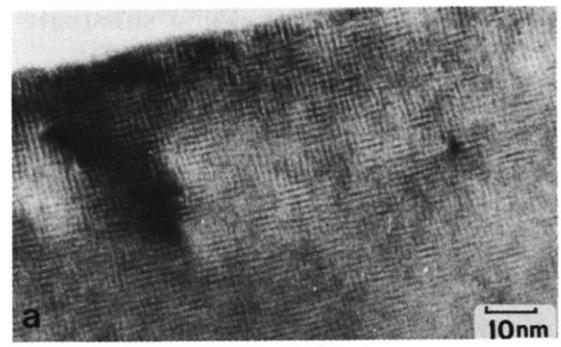

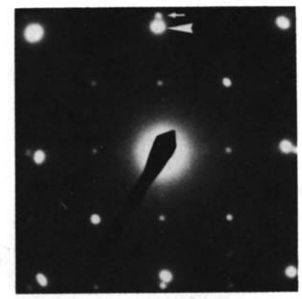

Fig. 3. (a) The HREM images show, that the $3a_p$ superstructures are established forming the tetragonal phase with a frequent change of the superstructure direction which leads to a "marquetry-like" contrast; (b) The E.D. pattern gives evidence of weak $3a_p$ extra spot (small white triangles) and sometimes of a small rotation with respect to the MgO matrix (small white arrow).

Moreover the $\vec{a}$ (or $\vec{b}$) and $\vec{c}$ axis are rotated with respect to the initial tetragonal domains. The measurements of the parameters taking MgO as reference show that there exists a systematical correlation between the misorientation of the grains and the amplitude of the orthorhombic distortion. The significant mismatch between the tetragonal matrix and the orthorhombic phase shows clearly that the growth of the latter is not epitaxial. On the opposite the d_{110} distances, very similar in both structures, suggest that the tetragonal to orthorhombic transformation is topotactic, the tilting of the grains around $[1\bar{1}0]$ being a way for minimizing the mismatch between the parameters.

At this stage, the large domains exhibit widths up to several hundred angströms; they can be connected through boundaries which are generally parallel to $(100)_p$ or $(110)_p$ but generally as islands on the tetragonal "marquetry-like" structure (Fig. 5).

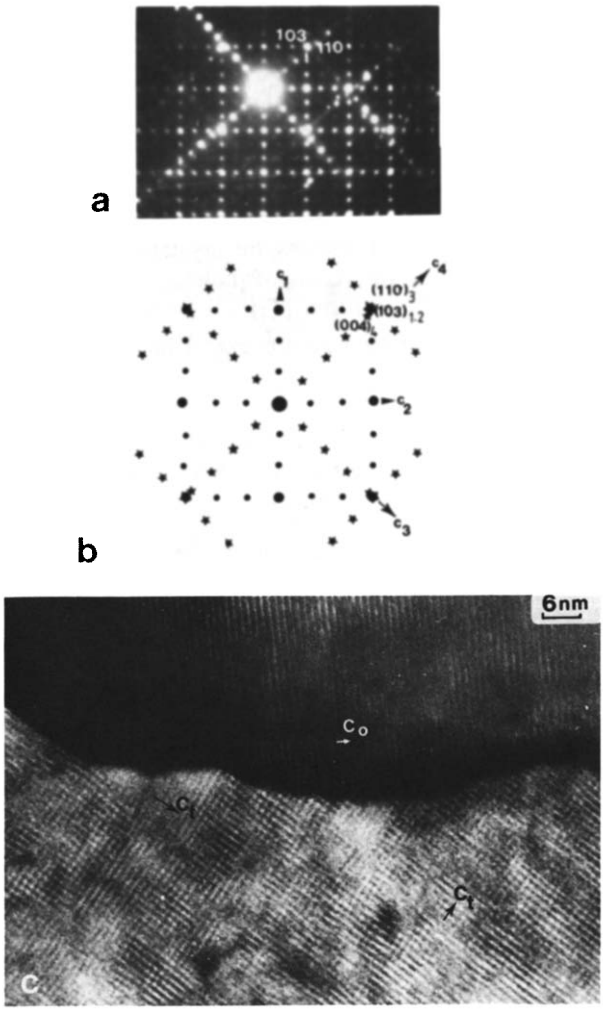

Fig. 4. The orthorhombic domains often exhibit a $[1\bar{1}0]$ orientation with respect to the tetragonal $\vec{a}$-axis phase. (a) The E.D. pattern shows the superposition of the two components (orthorhombic and tetragonal); (b) schematic drawing of the complex pattern. The reflections of the tetragonal pattern, indiced 1 and 2, are represented by black dots and those of the orthorhombic pattern, indiced 3 and 4, by stars. In both cases, domains with 90° oriented $\vec{c}$-axis are observed, labeled C_1 and C_2 for the tetragonal phase and C_3 and C_4 for the orthorhombic one. In the tetragonal systems, $(103)_1$ and $(103)_2$ are common reflections which are perfectly superposed to the $(110)_3$ reflection of one of the orthorhombic systems (in agreement with the evolution of the cells parameters). The $(004)_4$ reflection of the second orthorhombic system is close to these reflections but not superposed. (c) The corresponding image shows a large domaine of the orthorhombic phase ($\vec{c}$-axis is labeled c_0) rotated with respect to the tetragonal domain ($\vec{c}$-axis labeled c_1).

The overall images show that the films consist of rectangular but poorly welded grains. The corresponding E.D. pattern (Fig. 6) attest that the $\vec{a}$ axis is now perpendicular to the substrate, whereas $\vec{b}$ and $\vec{c}$ exhibit aleatory orientations in the substrate plane with regard to the MgO lattice.

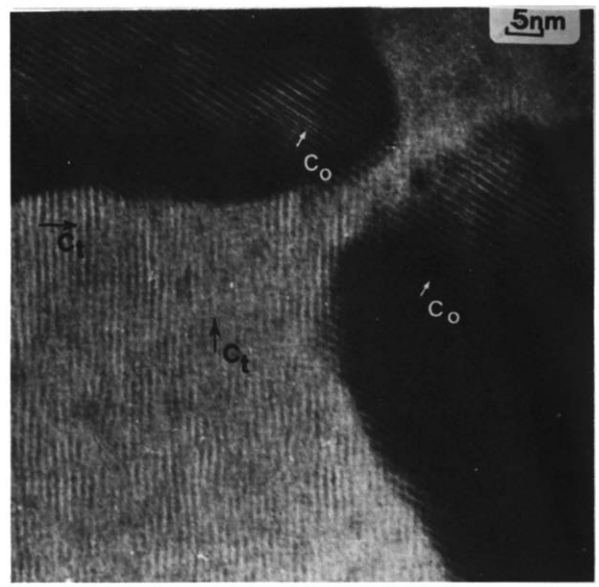

Fig. 5. Islands of orthorhombic domains, $[1\bar{1}0]$ oriented, appearing in the marquetry-like tetragonal structure.

The existence of an intermediate layer has been observed which is poorly crystallized. After cooling down to room temperature (1 hour from 750°C), the voids between the $\vec{a}$ axis oriented grains are filled up, leading to a perfect connection of the 90° "$\vec{b}$-$\vec{c}$" oriented domains.

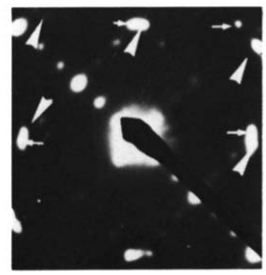

Fig. 6. The E.D. pattern show that the [100] plane of the 123 grains is parallel to the substrate, the b parameter of the perovskite exhibits an angle close to 50° with regard to the $\vec{a}$-axis of MgO.

At this stage the YBCO thin film is optimized (Fig. 7) and exhibit a very sharp transition with a T_C (R = 0) of 89 K (Fig. 8).

It is important to outline that when the 750°C plateau of the temperature profile scan is prolonged, very large grain are observed with a $\vec{c}$-axis orientation perpendicular to the substrate and misoriented with regard to the MgO lattice [12].

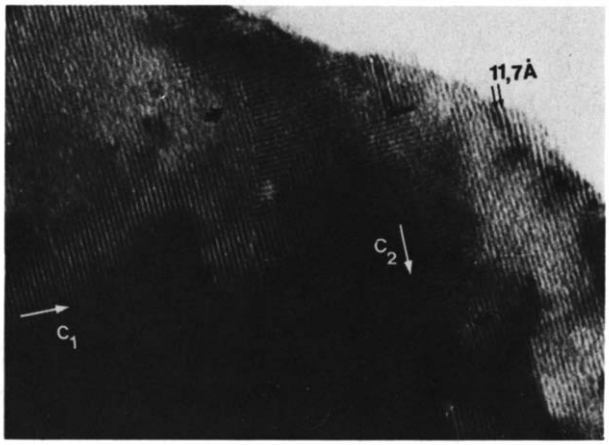

Fig. 7. [100] bright field image of the $\vec{a}$-axis optimized film of YBCO after slow cooling.

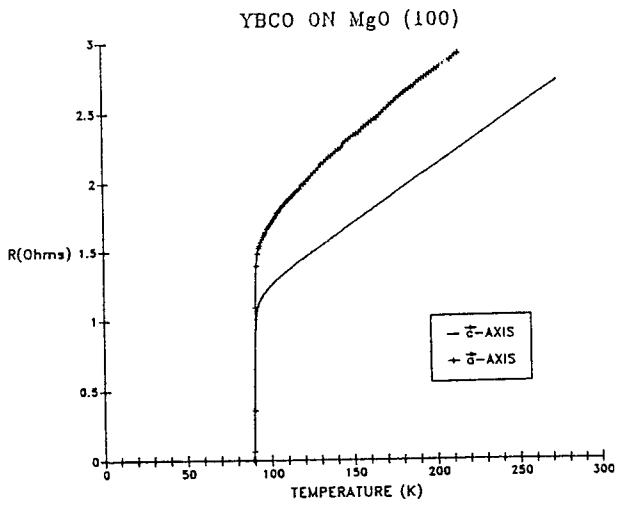

Fig. 8. Resistive transition for $\vec{a}$-axis and $\vec{c}$-axis oriented YBCO films on MgO.

3. Conclusion

This work shows that YBCO $\vec{a}$ axis oriented thin films can be deposited on (001) MgO substrate. The absence of an epitaxial process appears as reasonable if we consider the mismatch between the two cells and is the result of a complex mechanism. The role of the intermediate layer is not well understood owing to the lack of data such as the thickness, the crystallinity state or the chemical composition. Nevertheless, the physical characteristics of these films [$T_{(R = 0)}$ = 89 K] can be compared to these observed on $\vec{c}$ axis films grown on MgO substrates.

Now, the next step for this study is the deposition of an $\vec{a}$ axis oriented heterostructure (S.N.S.) on MgO substrates in order to realize Josephson junctions.

References

1 D. Dijkkamp, T. Venkatesan, X.D. Wu, S.A. Shaheen, N. Jinawi, Y.H. Minke-Lee, W.L. McLean and M. Croft, Appl. Phys. Lett. 51 (1987) 619.
2 J. Fröhlingsdorf, W. Zander ans B. Stritzker, Solid State Commun. 67 (1988) 965.
3 B. Roas, L. Schultz and G. Endres, Appl. Phys. Lett. 53 (1988) 1557.
4 X.D. Wu, A. Inam, T. Venkatesan, C.C. Chang, E.W. Chase, J.M. Tarascon and B. Wilkens, Apll. Phys. Lett. 52 (1988) 754.
5 X.X. Xi, G. Linker, O. Neyer, E. Nold, B. Obst, F. Ratjel, R. Smithey, Strehlan, F. Wescherfelder and J. Geerk, Z. Phys. B 74 (1989) 13.
6 A. Inam et al., ICMAS 91. IITT-International editor.
7 A. Inam, C.T. Rogers, R. Ramesh, K. Remsching, L. Farrow, D. Hart, T. Venkatesan and B. Wilkows, Appl. Phys. Lett. 57 (1990) 2484.
8 J.B. Barner, C.T. Rogers, A. Inam, R. Ramesh and S. Bersey, Appl. Phys. Lett. 59 (1991) 1383).
9 T. Hase, H. Takahashi, H. Izumi, K. Omata, K. Suzuki, T. Morismita and S. Takana, J. Cryst. Growth 115 (1991) 788.
10 J.F. Hamet, B. Mercey, M. Hervieu and B. Raveau, Physica C 193 (1992) 465.
11 V. Caignaert, M. Hervieu, J. Wang, G. Desgardin, B. Raveau, F. Botterel and J.M. Haussonne, Physica C 170 (1990) 139.
12 J.F. Hamet, B. Mercey, M. Hervieu, G. Poullain and B. Raveau, Physica C 198 (1992) 293.